Reaction Kinetics, Mechanisms and Catalysis (2023) 136:2441–2463
https://doi.org/10.1007/s11144-023-02475-z

C–H activation of ethane on palladium clusters: a computational study at the dual levels of density functional theory and coupled-cluster theory

Samuel L. Montgomery[1] · **Yingbin Ge**[1]

Received: 17 July 2023 / Accepted: 12 August 2023 / Published online: 19 August 2023

Abstract

We studied the C–H activation of ethane on the palladium (Pd) atomic clusters at the CCSD(T)/TZ//B3LYP/DZ level of theory, where TZ and DZ denote the LANL2 valence triple-ζ and double-ζ basis sets that include a relativistic pseudopotential for the Pd core electrons. In this study, we globally optimized first the Pd_n clusters ($n = 1$–8) and then the transition state (TS) structures of $Pd_n + C_2H_6 \rightarrow H{-}Pd_n{-}C_2H_5$. For each cluster size, we studied four spin states ($S = 0$, 1, 2, 3). The Pd atom is in the singlet electronic state ($[Kr]4d^{10}$) at the CCSD(T) level. The CCSD(T) global minima of the Pd_3, Pd_7, and Pd_8 clusters are also in the singlet electronic state, whereas the CCSD(T) global minima of Pd_2, Pd_4, Pd_5, and Pd_6 are in the triplet electronic state. The atomization energy of Pd_n increases monotonically with the cluster size. Pd_4 and Pd_6 are particularly stable relative to their neighboring sizes. Among all sizes, Pd_4 is the least active toward the C–H bonds in ethane, followed by sizes 5, 7, 3, and 1, whereas Pd_2, Pd_6, and Pd_8 are the most active: the enthalpy of activation of the $Pd_n + C_2H_6 \rightarrow H{-}Pd_n{-}C_2H_5$ reaction at room temperature are –29, –21, and 8 kJ/mol at these three sizes, respectively, indicating their strong ability to activate ethane. Among these three sizes, Pd_2 is highly unstable and thus less ideal. Pd_6 and Pd_8 are both energetically stable and active toward the C–H bonds of ethane.

Keywords Palladium · Ethane · Ethene · Dehydrogenation · B3LYP · CCSD(T)

Introduction

Every year more than 100 million tons of ethylene are produced from ethane [1]. The rate-limiting step of the conversion from ethane to ethene involves the C–H bond breaking in ethane. The energy barrier of this rate-limiting step can

✉ Yingbin Ge
yingbin@cwu.edu

[1] Department of Chemistry, Central Washington University, Ellensburg, WA 98926, USA

be reduced by using catalysts that effectively weaken or break a C–H bond in ethane. Considering the magnitude at which this reaction occurs, it is significant to investigate new catalysts to further bring the energy barrier down. Lowering the energy barrier for breaking a C-H bond in ethane, even by only a few kJ/mol, could potentially be valuable. Therefore, numerous efforts have been made to find novel catalysts to break the C–H bond more easily [2–36]. We have also been studying the atomic clusters of various transition metals (TM) as potential catalysts for the production of ethene via the oxidative dehydrogenation (ODH) of ethane (the catalytic cycle is depicted in Fig. 1) [15, 22, 23].

In our previous density functional theory (DFT) studies on the abilities of the Pt, Ir, and Rh atomic clusters to break a C–H bond in ethane (and propane) [15, 22, 23], several common features were observed. In all three cases, the C–H bond is weakened and eventually broken by the transition metal cluster, not because the d electrons of the TM cluster flow into the σ* bonding orbital of ethane, but because the σ bonding electrons in ethane flow into an empty d orbital of the transition metal cluster. The direction of the electron flow is evidenced directly by the Mulliken charge analysis; this is also evidenced indirectly by the correlation between the catalytic ability of a TM cluster and the diffusiveness of its LUMO that can accept electrons from ethane. In addition, we compared the TM cluster-mediated bond breaking in ethane and propane: the additional electron-pushing methyl group in propane lowers the energy barrier of the C–H bond cleavage. This substituent effect supports our conjecture that the C–H bond is weakened or broken by the Pt/Ir/Rh clusters because these TM clusters have empty d orbitals that readily accept the σ bonding electrons of ethane. In addition, we found that the natural bond orbital (NBO) charges [37, 38] and Wiberg bond indexes (WBIs) [39–41] may serve as reliable tools for prescreening of the various catalytic sites on the Ir and Rh clusters, and potentially other similar transition metal (e.g., Pt) clusters that activate the C–H bonds of ethane and other light alkane [23].

After the Pt/Ir/Rh clusters were studied, Pd, the remaining element in the 2×2 square of ^{45}Rh, ^{46}Pd, ^{77}Ir, and ^{78}Pt in the periodic table is studied with a focus on its atomic clusters' thermal stability and activity toward ethane. The ground state electron configurations of Rh, Pd, Ir, and Pt are [Kr]4d^{8}5s^1, [Kr]4d^{10}, [Xe]4f^{14}5d^{7}6s^2,

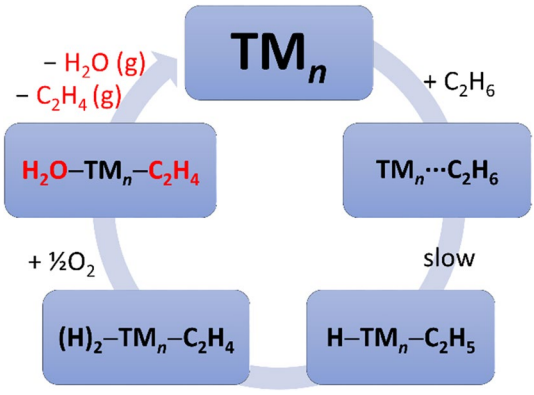

Fig. 1 The catalytic cycle of the ODH of ethane. The step labeled "slow" is the presumably rate-limiting step of the catalytic cycle. Molecular formulas in red font are either vibrationally energetic in the TM complex or translationally energetic in the gas phase

and $[Xe]4f^{14}5d^{9}6s^{1}$, respectively. Pd is special because, among these four elements, the Pd atom is the only one with completely filled d orbitals and thus may lack the ability to accommodate the σ bonding electrons of ethane. Since every subshell of the Pd atom is either completely filled or completely empty, it would be interesting to see how Pd atoms form metallic bonds between each other and how the Pd clusters interact with ethane. While numerous computational studies of the Pd atomic clusters or Pd-containing bimetal alloys and their interactions with hydrocarbons have been performed and published, most of these studies, if not all, have their accuracy levels limited by the computational methods, typically DFT methods that may not describe dispersion accurately, in their studies [42–50]. Therefore in this study, we used the B3LYP method coupled with Grimme's empirical dispersion to obtain the optimized structures of the Pd clusters and the transition states (TS) for the Pd cluster-mediated C–H bond-breaking reactions. For an enhanced level of accuracy, we further used the "gold standard" of computational chemistry, the CCSD(T) method, to study the energetics of the Pd clusters and their reactions with ethane. The ideal sizes of the Pd atomic clusters were then proposed based on a balance between their energetic stability and activity toward ethane.

Computational methods

The B3LYP hybrid GGA method [51–53] was used in this study to carry out the optimization and frequency calculations of the Pd atomic clusters and the transition states (TS) of the $Pd_n + C_2H_6 \rightarrow H-Pd_n-C_2H_5$ reactions. The D3 empirical dispersion formulated by Grimme with Becke–Johnson damping [54] (D3BJ) was included in the B3LYP calculations. Hereafter, this computing scheme is denoted by B3LYP-D3BJ. The vibrational frequency calculations ensure that the Pd_n local minima have zero imaginary frequencies, whereas every TS structure has exactly one imaginary frequency that involves the interaction between the Pd cluster and a C–H bond of ethane. Some highly symmetric Pd_n structures such as the linear Pd_3 and the square planar Pd_4 were found to have one or even more imaginary frequencies. The intrinsic reaction coordinate (IRC) calculations, a.k.a. the minimum energy path (MEP) calculations, were carried out to ensure that each identified transition state connects the reactants ($Pd_n + C_2H_6$) and the desired product ($H-Pd_n-C_2H_5$).

In the B3LYP-D3BJ optimization and frequency calculations, polarized valence double-ζ basis sets were used. The LANL2DZ basis set and the LANL2 effective core potential (ECP) [55], augmented with f-type polarization functions [56], were employed on the Pd atoms. The polarized valence double-ζ 6-31G(d) basis sets were employed on the C, H, and O atoms [57, 58]. Hereafter, this combination of the valence double-ζ basis sets is denoted by DZ. Overall this B3LYP-D3BJ/DZ computing scheme used in the optimization, frequency, and IRC calculations is the same as or very similar to those used in our previous studies on the C–H activation by the Pt, Ir, and Rh atomic clusters [15, 22, 23]; it is also similar to Liu et al.'s calculations on the functionalization of C-H bonds [59]. The natural bond orbital (NBO) [37, 38] analysis was carried out using version 3.1 of the NBO program [60].

The CCSD(T) single-point energy calculations were carried out on the B3LYP-D3BJ/DZ structures to achieve a higher level of accuracy. In the CCSD(T) calculations, The valence triple-ζ LANL2TZ basis set and the LANL2 effective core potential (ECP) [55], augmented with f-type polarization functions [56], were employed on the Pd atoms. The polarized valence triple-ζ 6-311G(d) basis sets were employed on the C, H, and O atoms [57, 58]. Hereafter, this well-balanced combination of valence triple-ζ basis sets is denoted by TZ. The CCSD(T) computing scheme is denoted by CCSD(T)/TZ//B3LYP-D3BJ/DZ or simply CCSD(T)//B3LYP in short for visual clarity. The 298 K internal energy, 298 K enthalpy (H), and 298 K Gibbs free energy (G) presented in this study are the sums of the CCSD(T)/TZ single-point electronic energy and the corresponding thermal corrections calculated at the B3LYP-D3BJ/DZ level of theory.

For the smallest Pd_2 and Pd_3 clusters, we were able to carry out the geometry optimization calculations at the CCSD(T)/TZ level to compare the CCSD(T)/TZ and B3LYP-D3BJ/DZ optimized structures. The CCSD(T) optimization calculations were completed numerically due to the lack of analytical gradients at the CCSD(T) level of theory. We also used the double-differentiation numerical method to obtain the CCSD(T) vibrational frequencies of the Pd_2 clusters in the singlet and triplet electronic states.

The B3LYP and other DFT calculations were carried out with the Gaussian 09 program (Windows version) [61]. The CCSD(T) calculations were carried out with the Gaussian 16 program (Linux version) [62].

Results and discussion

CCSD(T)/TZ vs B3LYP-D3BJ/DZ

In this study, we compared the performance of the hybrid and pure DFT methods against the CCSD(T) benchmark and also against the experimental data (0.81 eV) [63] of the singlet–triplet (S-T) gap of the Pd atom. The S-T gap is simply the energy of the triplet electronic state of the Pd atom minus its energy in the singlet electronic state. Table 1 shows the comparison of the S-T gap of the Pd atom using the hybrid B3LYP and the pure BLYP DFT methods, along with the CCSD(T) method. Two different basis sets were used in the calculations: a smaller double-ζ LANL2DZ(f) basis set and a larger triple-ζ LANL2TZ(f) basis set. The table shows that as the basis set size increases, the calculated singlet–triplet gap decreases. The difference between the BLYP and B3LYP results is negligible (0.83 vs. 0.83 eV) when the double-ζ basis set is used but becomes more appreciable (0.72 eV vs. 0.69 eV) when the larger triple-ζ basis set is used. Among all these computing schemes, the B3LYP and BLYP calculations with the smaller DZ basis set result in the smallest discrepancies (only 0.02 eV) from the experimental value. Overall, the B3LYP values are even slightly more accurate than the CCSD(T) calculations with either the smaller DZ or the larger TZ basis set. In theory, the higher-level CCSD(T) method should be more accurate than the DFT methods when an infinitely large basis set is used. Therefore, the better performance of the B3LYP/DZ method is likely due

Table 1 CCSD(T) and DFT calculated energies of the singlet and triplet Pd atom and the singlet–triplet (S-T) gap

	CCSD(T)		B3LYP		BLYP	
Basis set	DZ	TZ	DZ	TZ	DZ	TZ
^{1}Pd (a.u.)[a]	−126.0780	−126.1200	−126.7068	−126.7075	−126.6138	−126.6155
^{3}Pd (a.u.)	−126.0470	−126.0941	−126.6761	−126.6811	−126.5831	−126.5900
S-T gap (eV)	0.84	0.71	0.83	0.72	0.83	0.69
Error[b] (eV)	0.03	−0.10	0.02	−0.09	0.02	−0.12

[a]1 a.u. = 27.2114 eV = 2625.50 kJ/mol

[b]The errors were calculated against the experimental value (0.81 eV)

to a fortuitous cancelation of errors for the studied system. Nonetheless, based on its agreement with experimental values of the S-T gap of the Pd atom as well as its success in the previous studies of the Ir and Rh systems [15, 23], we are sufficiently confident in using the B3LYP-D3BJ/DZ method for the geometry optimization and vibrational frequency calculations of the Pd clusters in this study.

Fig. 2 shows the 23 atomic structures of Pd_n ($n = 3-8$) we optimized at the B3LYP-D3BJ/DZ level of theory. The structures of the Pd atom and the Pd_2 dimer were not included in the figure because of their simplicity. For Pd_3, the triangular and linear structures were locally optimized. For sizes larger than 3, linear structures are no longer studied due to their much higher energies [64]. For Pd_4, the rhombus, square planar, and tetrahedral structures were optimized. Because the planar structures of Pd_4 are much less stable than the nonplanar structures [64], planar structures were no longer considered beyond size 4. For Pd_5, the square pyramidal and trigonal bipyramidal structures were optimized. For Pd_6, the fused bi-tetrahedron, capped square pyramidal, trigonal prism, elongated/compressed octahedral, and octahedral structures were optimized. For Pd_7, the capped trigonal prism, capped octahedral structures, and pentagon bipyramidal structures were optimized. For Pd_8, the bicapped octahedral structure, the cubic structure, and various distorted cubic structures were optimized. In general, the choices of the initial structures of the Pd clusters were based on several previous studies [48, 64, 65].

For each atomic cluster structure, four different electronic structures with $S = 0$, 1, 2, 3 were studied, where S is the electron spin quantum number. The $S = 3$ spin states with six unpaired electrons were found to be highly unstable and therefore higher than $S = 3$ spin states were not examined in this study. The ground electronic state of the Pd atom is a singlet at the B3LYP and CCSD(T) levels. In partial agreement with some previous DFT studies [46, 48, 50, 64, 65], we found the CCSD(T) global minima of the Pd clusters are in a singlet electronic state at sizes 3, 7, and 8, whereas the global minima of Pd_2, Pd_4, Pd_5, and Pd_6 are in the triplet electronic state. It was experimentally verified that the global minimum of Pd_2 is indeed in the triplet state [66, 67]. Our CCSD(T) predicted spin states of the Pd_n global minima agree with the BLYP study [48] but differ from the PW91 DFT calculations by Zhang et. al. [64], which suggest that the Pd_n global minima are all in the triplet electronic states

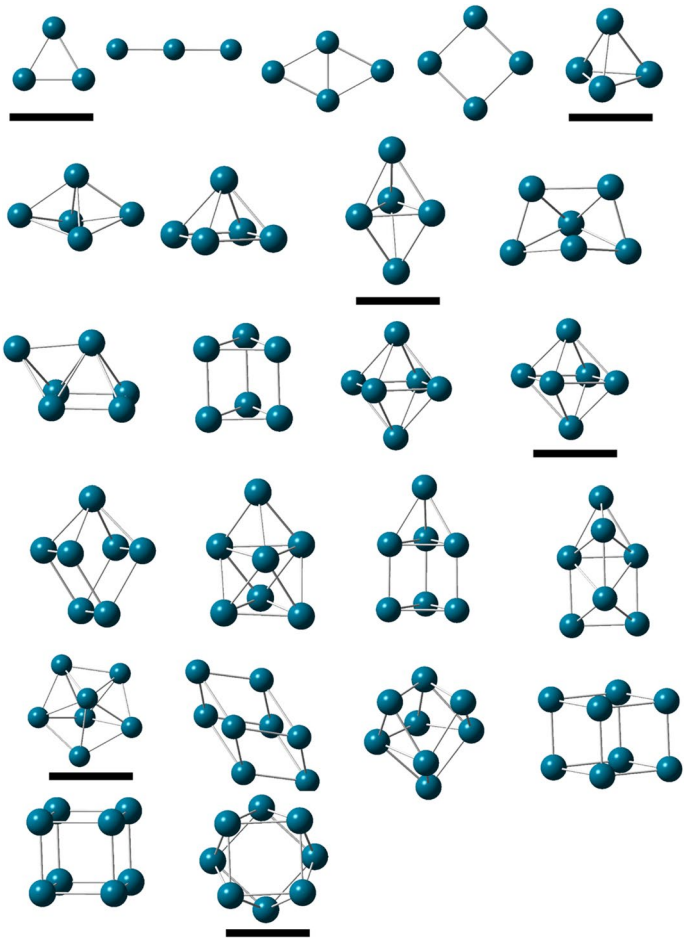

Fig. 2 Optimized structures of Pd_n clusters ($n=3-8$). The CCSD(T) global minimum structures are underscored. The spin quantum number S is 1 for sizes 2, 4, 5, and 6; S is 0 for all other sizes

except that Pd_8 is in the singlet state [64]. Interestingly, another PW91 study conducted by Luo et. al. [50] suggests that Pd_3 and Pd_6 global minima are in the singlet electronic state whereas sizes 2, 4, 5, 7, and 8 are in the triplet electronic state. There are two reasons why these two PW91 studies made different predictions regarding the spin states of the Pd_n global minima. One reason is that they used different basis sets: Zhang et al. used a plane wave basis set [64], whereas Luo et al. used a double numerical basis set [50]. Another reason is that the energy spacings between the Pd_n global and local minima are typically so small that slightly different computing schemes (e.g., different basis sets) may result in different energy rankings. Nonetheless, the atomic structures of the Pd_n global minima at the CCSD(T) level are the same as those proposed by Zhang et al. [64] and very close to those proposed by Luo et al. [50]. From size 3 to size 8, the global minimum structures at both the

CCSD(T) and PW91 [64] levels of theory are triangular, tetrahedral, trigonal bipyramidal, nearly octahedral, pentagonal bipyramidal, and twisted cubic (in which the bottom square of the cube is rotated 45 degrees about the vertical axis). The PW91 study by Luo et. al. proposed the same global minimum structures for all sizes except for size 8: they suggest that the Pd_8 lowest-energy structure is a bicapped octahedron instead of a twisted cube. The CCSD(T) predicted Pd_n global minimum structures also agree with the BLYP [48] and BP86 [46] calculations in general. In these DFT studies, the global minimum structures of Pd_n ($n=3$–7) are also triangular, tetrahedral, trigonal bipyramidal, nearly octahedral, and pentagonal bipyramidal. Size 8 was not examined in the BLYP study [48] whereas the BP86 [46] calculations suggest that the Pd_8 global minimum is a bicapped octahedron. Overall, the PW91, BP86, and BLYP DFT methods predicted the same lowest-energy structures as our CCSD(T)//B3LYP-D3BJ method with very few exceptions [46, 48, 50, 64]. While the prior DFT calculations and our CCSD(T) calculations do not completely agree on the spin states of the Pd_n global minima, we are more confident with our CCSD(T) predictions for two reasons: one is that we included Grimme's empirical dispersion in the DFT calculations to obtain more accurate optimized structures; the other is that the CCSD(T) method we used in this study is widely accepted as the gold standard of computational chemistry and is typically more accurate and reliable than the DFT methods both in theory and in practice.

We then studied these Pd atomic clusters' abilities to activate a C–H bond in ethane. The 19 studied TS atomic structures of the $Pd_n + C_2H_6 \rightarrow H{-}Pd_n{-}C_2H_5$ reactions ($n=1$–8) are shown in Fig. 3. Fewer TS structures than the Pd_n structures are presented because the TS search starting from two different Pd_n structures may result in the same TS structure. For example, when a planar Pd_4 atomic cluster inserts into a C-H bond of ethane, the four Pd atoms always become non-planar (nearly tetrahedral) in the TS structure. For each TS structure, four spin states ($S=0$–3) were studied. The lowest-energy TS structures for nearly all sizes adopt the singlet electronic state ($S=0$) except for size 7 ($S=1$). This is likely because the introduction of ethane into the system breaks the high symmetry of the molecular orbitals (MOs) of the Pd atomic clusters and eliminates the (near) degeneracy of the MOs of the Pd clusters; the energy spacings between adjacent MOs become so large that the electrons occupy the lowest possible MOs, two by two, dictated by the Aufbau principle. As expected, the $S=3$ high spin state of every TS structure has much higher energy than all other spin states in all cases. This is because too many electrons are forced to occupy high-energy MOs in the $S=3$ electronic state. This energy increase cannot be sufficiently compensated by the energy decrease due to the extra negative exchange energy and the smaller e-e repulsion in the high-spin state. For this reaction, no higher spin state than $S=3$ is of interest or further examined in this study.

Fig. 4 compares the CCSD(T)/TZ and B3LYP-D3BJ/DZ electronic energies for the Pd clusters (4a) and the TS structures (4b). The correlation is nearly perfect with $R^2=1$ in both cases. The CCSD(T) energy is approximately 99.53% of the B3LYP-D3BJ energy for Pd atomic clusters and 99.55% for the TS structures. The very small 0.02% difference in percentage is mostly due to the introduction

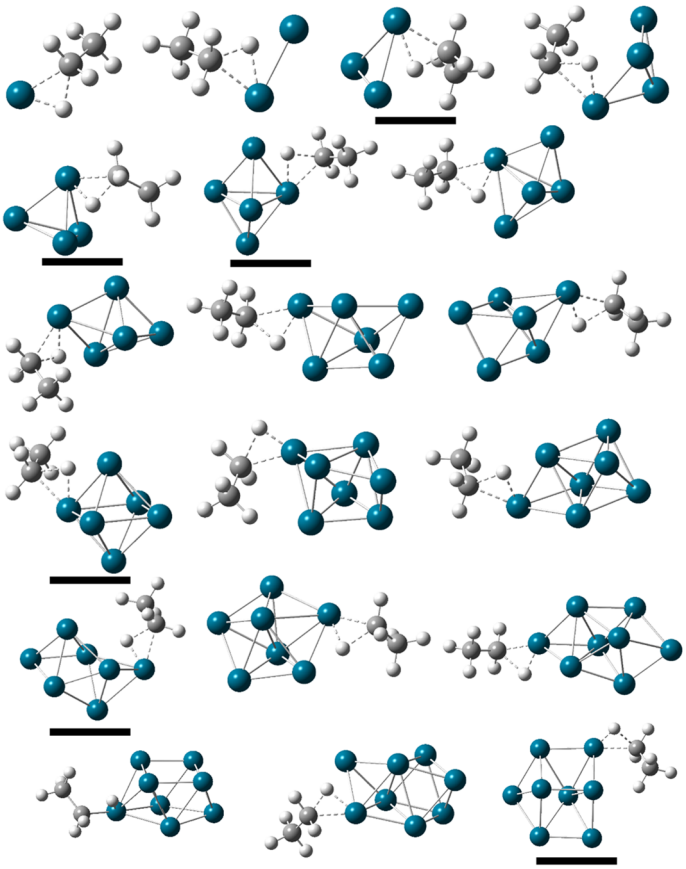

Fig. 3 The optimized TS structures of the $Pd_n + C_2H_6 \rightarrow H-Pd_n-C_2H_5$ reactions ($n = 1$–8). The CCSD(T) global minimum structures are underscored. The spin quantum number S is 1 for size 7 and 0 for all other sizes

of ethane in the TS structure. The CCSD(T)/TZ singlet point energy of a free ethane molecule is 99.73% of its B3LYP-D3BJ/DZ energy.

The correlations between the CCSD(T) and B3LYP-D3BJ energies are virtually perfect partly because of the vast difference in energy between the Pd clusters of different sizes. Therefore, we also compared the energy per Pd atom for all cluster sizes in Fig. 5. For the TS structures, we first subtract the energy of free ethane from the total energy, and then divide the remaining energy by the number of Pd atoms.

Fig. 5 demonstrates satisfactory linear correlations between the CCSD(T) and B3LYP-D3BJ energies per Pd atom. The CCSD(T) energy per Pd atom is 99.53% of the B3LYP/D3BJ energy in both Pd atomic clusters and in TS structures (the energy of free ethane is subtracted from the TS energy). The correlation between the CCSD(T) and B3LYP-D3BJ results for the TS structures ($R^2 = 0.9926$) is notably

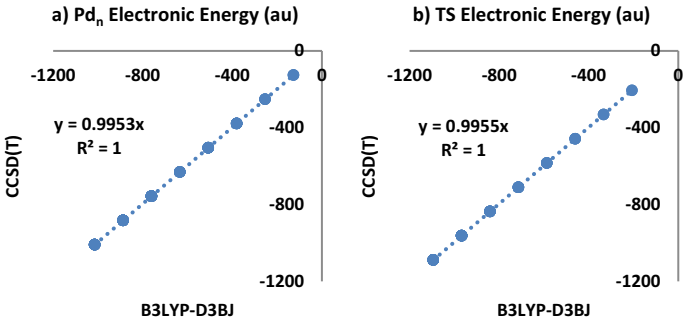

Fig. 4 CCSD(T)/TZ vs B3LYP/DZ electronic energies for **a** the Pd_n atomic clusters and **b** the TS structures of the $Pd_n + C_2H_6 \rightarrow H - Pd_n - C_2H_5$ reactions

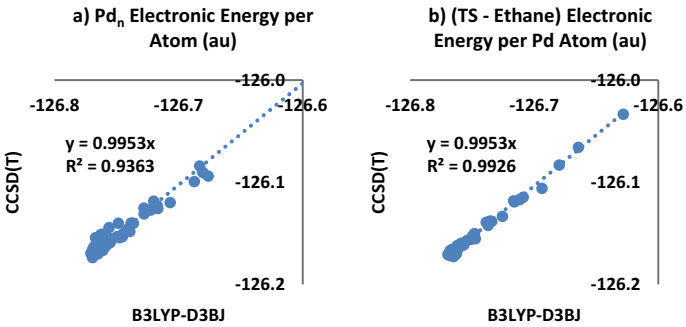

Fig. 5 CCSD(T)/TZ vs B3LYP/DZ electronic energies per Pd atom for **a** the Pd_n atomic clusters and **b** the TS structures (the ethane energy is subtracted)

stronger than that for the Pd clusters ($R^2 = 0.9363$). This is because the near degeneracy among multiple electronic states and the resulting spin contamination prevalent in the Pd atomic clusters are suppressed in the TS structures due to the introduction of the ethane. As expected, less spin contamination in the TS structures results in a better correlation between the density functional theory and the coupled cluster theory. The strong correlation between the CCSD(T)/TZ and B3LYP-D3BJ/DZ energies, in total or per Pd atom, serves as indirect evidence of the satisfactory accuracy of the B3LYP-D3BJ optimized geometries. We further compared the CCSD(T)/TZ and B3LYP-D3BJ/DZ optimized structures for Pd_2 in the singlet and triplet electronic states. For the singlet electronic state, the CCSD(T)/TZ and B3LYP-D3BJ/DZ bond lengths are 2.820 and 2.764 Å, respectively. Compared to the benchmark CCSD(T)/TZ result, the B3LYP-D3BJ/DZ method underestimates the bond length by 0.056 Å. Note that the CCSD(T)/TZ bond distance of Pd_2 in the singlet electronic state (2.820 Å) is longer than the Pd–Pd distance in the face-centered cubic (FCC) crystalline structure of bulk Pd (2.748 Å) [68], which suggests an unusually weak bond in the Pd dimer in the singlet electronic state. For the triplet electronic state,

the CCSD(T)/TZ and B3LYP-D3BJ/DZ bond lengths are 2.506 and 2.554 Å, respectively. Compared with the experimental bond length (2.48 Å) [69], the CCSD(T)/TZ and B3LYP-D3BJ/DZ methods overestimate the bond length by 0.026 and 0.074 Å, respectively. Others' PW91, B3LYP, and BLYP calculations also overestimated the Pd–Pd bond distance by 0.01 [64], 0.06 [48], 0.05 [70], and 0.08 Å [71]. The PW91 [64] and CCSD(T) bond distances are more accurate than some other DFT calculations [48, 70, 71] and our own B3LYP-D3BJ calculations for the Pd dimer in the triplet electronic state. The discrepancies between the CCSD(T) and B3LYP-D3BJ bond distances (2.506 vs. 2.554 Å) of the Pd dimer do not significantly impact the accuracy of the CCSD(T) electronic energy: the CCSD(T)/TZ optimized energy is merely 0.4 kJ/mol or 0.8 kJ/mol lower than the CCSD(T)/TZ//B3LYP-D3BJ/DZ energy for the singlet or triplet electronic state, respectively. Both CCSD(T)/TZ and B3LYP-D3BJ/DZ calculations suggest that the Pd–Pd bond distance in the triplet state is significantly shorter than that of the singlet electronic state. This is because the theoretical Pd–Pd bond order is one in the triplet electronic state but zero in the singlet electronic state (see reasoning in "The Pd_n atomic clusters").

We also compared the CCSD(T)/TZ and B3LYP-D3BJ/DZ optimized structures for Pd_3 in the singlet and triplet electronic states. For the singlet electronic state, the CCSD(T)/TZ and B3LYP-D3BJ/DZ optimized structures are both equilateral triangles (D_{3h} point group) with a bond length of 2.531 and 2.509 Å, respectively. The B3LYP-D3BJ/DZ method slightly underestimates the bond length by 0.022 Å. For the triplet electronic state, the CCSD(T)/TZ and B3LYP-D3BJ/DZ structures are not equilateral triangles but isosceles triangles (C_{2v} point group) due to the Jahn–Teller effect. The CCSD(T)/TZ bond lengths are 2.596, 2.596, and 2.496 Å, whereas the B3LYP/DZ bond lengths are 2.573, 2.573, and 2.566 Å. The discrepancies between the CCSD(T) and the B3LYP/DZ bond lengths of Pd_3 (− 0.023, − 0.023, and 0.070 Å) do not significantly affect the accuracy of the CCSD(T) single-point energy either: the CCSD(T)/TZ optimized energy is only 0.5 kJ/mol or 1.9 kJ/mol lower than the CCSD(T)/TZ//B3LYP-D3BJ/DZ energy for the singlet or triplet electronic state, respectively.

The Pd_n atomic clusters

To understand the size effect on the energetics of these Pd clusters, we computed the atomization energy of these clusters with $S=0$, 1, 2, 3 at the CCSD(T)/TZ level of theory. The Pd atom in the ground electronic state ($[Kr]4d^{10}5s^0$) is used as the zero reference in the calculation of atomization energies. Although multiple atomic structures, each with multiple electronic spin states, were calculated, only the maximum atomization energies per atom of the Pd clusters for each cluster size, and the corresponding second derivatives with respect to the cluster size, are shown in Fig. 6 for visual clarity. The singlet electronic state ($S=0$) has the maximum atomization energy for sizes 1, 3, 7, and 8. Sizes 2, 4, 5, and 6 prefer the triplet state ($S=1$). The lowest-energy structures of $Pd_{3\text{-}8}$ adopt triangular, tetrahedral, square pyramidal, octahedral, pentagonal bipyramidal, and twisted cubic shapes, respectively. The expression of the energy second derivative for size n is $[E(n+1)+E(n-1)-2E(n)]$.

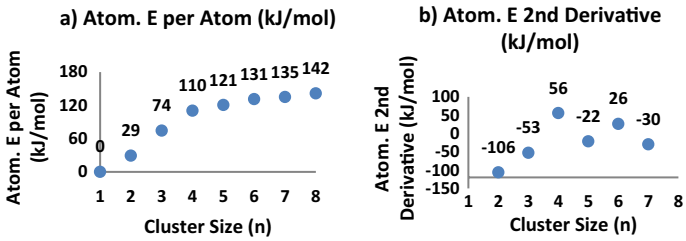

Fig. 6 **a** Atomization energies per atom, abbreviated as Atom E., of the Pd atomic clusters, **b** the atomization energy second derivatives with respect to the atomic cluster size

A positive energy second derivative indicates energetic stability relative to the nearest neighboring sizes because the disproportionation reaction $2Pd_n \rightarrow Pd_{n-1} + Pd_{n+1}$ is endothermic and thus less likely to occur at a finite temperature, whereas a negative second derivative indicates energetic instability relative to the nearest neighboring sizes.

Fig. 6a shows that the atomization energy per atom increases monotonically with the cluster size as expected because the average number of bonds increases as the average number of surrounding Pd atoms increases as the cluster size increases. We were not able to calculate the energy second derivative for size 1 or 8 because they each have only one nearest neighbor in cluster size. In agreement with a global optimization study at the BLYP level [49], sizes 2, 3, 5, and 7 have negative second derivatives and thus are energetically unstable relative to their nearest neighbors. Pd_2 is particularly unstable with the smallest atomization energy (29 kJ/mol) and the most negative energy second derivative (− 106 kJ/mol) at the CCSD(T) level.

Pd_4 and Pd_6 have a positive second derivative (56 and 26 kJ/mol, respectively) and are relatively stable. Specifically, size 4 might be considered the magic number of the small Pd clusters as Pd_4 has the largest energy second derivative. Although we cannot calculate the energy second derivative for Pd_8, the aforementioned global search at the BLYP level suggests that this size is also relatively stable [49].

Our CCSD(T) calculations suggest that $^1Pd_3$ has much larger atomization energy per atom than $^3Pd_2$ (74 vs 29 kJ/mol), which agrees with the multi-reference singles plus doubles configuration interaction (MRSDCI) calculations for the Pd dimer and trimer [72]. The Pd dimer in the singlet electronic state ($^1Pd_2$) has even smaller atomization energy per atom (17 kJ/mol) than the triplet electronic state (29 kJ/mol). The very weak bond strength of $^1Pd_2$ can be well understood by visualizing its ten highest occupied MOs in Fig. 7.

Among the 10 highest occupied MOs of $^1Pd_2$ in Fig. 7, from the bottom up, there is one $\sigma_{d\text{-}d}$ orbital, two degenerate $\pi_{d\text{-}d}$ orbitals, two degenerate $\delta_{d\text{-}d}$ orbitals, two degenerate $\delta^*_{d\text{-}d}$ orbitals, two degenerate $\pi^*_{d\text{-}d}$ orbitals, and one $\sigma^*_{d\text{-}d}$ orbital. The bond order (B. O.) is zero in $^1Pd_2$ because the ten d orbitals from the two Pd atoms form five bonding orbitals and five corresponding antibonding orbitals, all of which are doubly occupied. Note that Pd_2 in the triplet electronic state ($^3Pd_2$) has a bond order of 1. This is because when an excited ^{3}Pd atom with two unpaired electrons ($[Kr]4d^95s^1$) interacts with the ^{1}Pd atom ($[Kr]4d^{10}$) in the ground electronic state

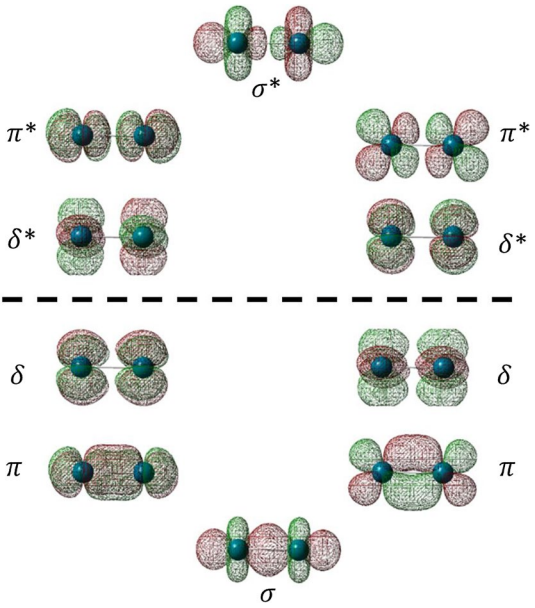

Fig. 7 The ten highest occupied MOs of $^1Pd_2$. The dashed line separates the five d-d antibonding MOs from the five d-d bonding MOs

to form $^3Pd_2$, the $\sigma_{4d\text{-}4d}$ and $\sigma_{5s\text{-}5\ s}$ bond orders are both one half and therefore the overall bond order of $^3Pd_2$ is one. The higher bond order of $^3Pd_2$ than that of $^1Pd_2$ is also evidenced by its higher CCSD(T) vibrational frequency (203 cm^{-1}) than that of $^1Pd_2$ (107 cm^{-1}). Note that a higher vibrational frequency indicates a larger force constant (k) and a deeper potential energy well (D_e). Note that the Tayler expansion of the Morse expression, $D_e(1 - e\text{^}{-}\alpha(r\text{-}r_e))^2$, suggests that the depth of the potential energy well of a diatomic molecule D_e is approximately proportional to its force constant k. While the Pd–Pd bond strength is anticipated to be much greater in the triplet electronic state (B. O. = 1) than in the singlet electronic state (B. O. = 0) in the Pd dimer, $^3Pd_2$ sits only 25 kJ/mol below $^1Pd_2$ in the potential energy surface (PES). This is because the bond energy of the $^3Pd_2$ is relative to a singlet Pd atom and a much higher-energy triplet Pd atom (^{3}Pd lies 68 kJ/mol higher than ^{1}Pd). Given the above data, we estimate the average strength of the $\sigma_{4d\text{-}4d}$ and $\sigma_{5s\text{-}5\ s}$ bonds between two Pd atoms is approximately 25 + 68 = 93 kJ/mol.

But if the Pd atoms in the ground singlet electronic state have only completely filled subshells, why can $^1Pd_3$ have a much larger atomization energy per atom (74 kJ/mol) than $^1Pd_2$ (17 kJ/mol) and even $^3Pd_2$ (29 kJ/mol)? The 15 highest occupied MOs of $^1Pd_3$ in Fig. 8 shed light: while 14 out of the 15 highest occupied MOs of $^1Pd_3$ are linear combinations of the d orbitals as expected, the HOMO, however, is a linear combination of three 5 s atomic orbitals, one from each Pd atom. The total bond order of $^1Pd_3$ is thus two. Both of these two bonds are three-center two-electron σ bonds, one being the overlap of three 5 s atomic orbitals and the other being the overlap of three 4d atomic orbitals. The latter results from the removal of the two electrons from the antibonding σ^*_{4d} orbital illustrated in Fig. 9. The empty σ^*_{4d} orbital (which is the LUMO of $^1Pd_3$) allows for the net σ bonding among the 4d orbitals (B. O. = 1) in $^1Pd_3$.

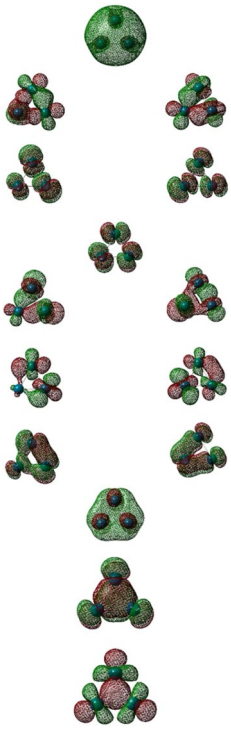

Fig. 8 The top 15 highest occupied molecular orbitals of $^{1}Pd_3$, among which 14 are interactions among the 4d orbitals, whereas the HOMO is the interaction among the 5 s orbitals

In addition, there is also net σ bonding among the 5 s orbitals (B. O. = 1) in $^{1}Pd_3$. Given the above data (the atomization energy per atom is 74 kJ/mol and the total bond order is 2), we estimate the average strength of the σ_{4d} and σ_{5s} bonds among the three Pd atoms in $^{1}Pd_3$ is approximately 74•3/2 = 111 kJ/mol, which is notably larger than that of $^{3}Pd_2$ (93 kJ/mol). This is because in a Pd dimer, each σ_{4d} or σ_{5s} bond results from only one region of constructive interaction between the two Pd atoms, while in a Pd trimer each σ_{4d} or σ_{5s} bond results from three regions of constructive interaction among the

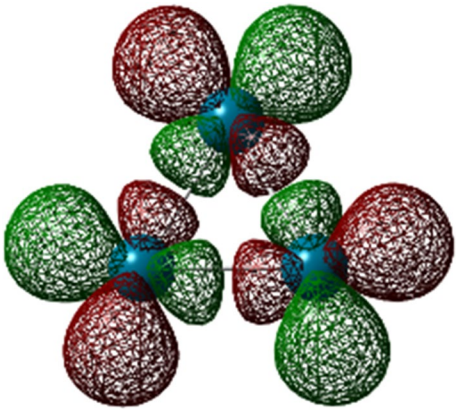

Fig. 9 The LUMO of $^{1}Pd_3$, an empty σ^{*}_{4d} orbital that allows for the net σ bonding among the 4d orbitals (B. O. = 1) in.$^{1}Pd_3$

three Pd atoms in a triangle. In general, the atomization energy per atom in a Pd cluster increases as the cluster size increases mainly because the number of neighboring Pd atoms increases on average. For comparison, each Pd atom is surrounded by 12 nearest Pd atoms in the face-centered cubic structure (FCC) structure of bulk Pd, which has significantly larger atomization per atom (377 kJ/mol) than the small clusters studied in this work [68].

The CCSD(T) global minimum of Pd_4 adopts a nearly tetrahedral structure (with slight distortion due to the Jahn–Teller effect) in the triplet electronic state with an atomization energy per atom of 110 kJ/mol. Its singlet counterpart ($^1Pd_4$) has a higher energy mainly because all d-d antibonding orbitals are fully occupied in $^1Pd_4$. The atomization energy per atom slowly increases as the cluster size increases from sizes 5 to 8: 121 kJ/mol, 131 kJ/mol, 135 kJ/mol, and 142 kJ/mol, respectively. Since these four values are still significantly smaller than the atomization energy per atom of bulk Pd (377 kJ/mol) [68], we suspect that the atomization energy per atom will continue to slowly increase well beyond size 8 and even well beyond size 55 as suggested by a PW91 study [64].

The TS of $Pd_n + C_2H_6 \rightarrow H–Pd_n–C_2H_5$

The internal energy (0 K), enthalpy (298 K), and Gibbs energy (298 K) of activation of the $Pd_n + C_2H_6 \rightarrow H–Pd_n–C_2H_5$ reactions are presented in Fig. 10. Their values along with the electronic energy of activation are also provided in Table 2.

The 0 K internal energy of activation (including the zero-point vibrational energy) is calculated using the following equation:

$$\Delta U^{\ddagger} = U(TS) - U\left(Pd_n\right) - U(\text{ethane}) \quad (1)$$

In this equation, U(TS) is the lowest possible internal energy of all TS structures optimized for the $Pd_n + C_2H_6 \rightarrow H–Pd_n–C_2H_5$ reaction for each cluster size n; $U(Pd_n)$ is the lowest possible energy of all Pd_n local minimum (LM) structures. Although other higher-energy TS structures and other higher-energy Pd_n structures also make contributions to the C–H activation by Pd clusters, Eq. 1 provides

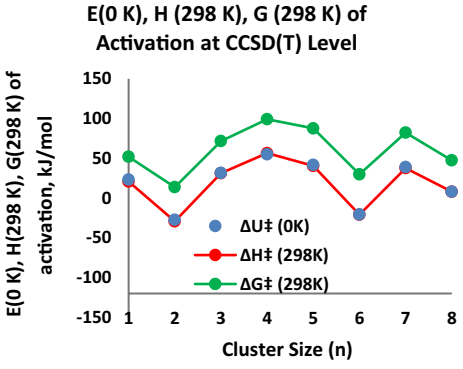

Fig. 10 The internal energy of activation at 0 K, enthalpy of activation at 298 K, and Gibbs energy of activation at 298 K at the CCSD(T)/TZ level

Table 2 The CCSD(T) electronic energy of activation, the internal energy of activation at 0 K, the enthalpy of activation at room temperature, and the Gibbs free energy of activation at room temperature. All values are in kJ/mol

n	$\Delta E_{elec}^{\ddagger}$	$\Delta U^{\ddagger}$ (0 K)	$\Delta H^{\ddagger}$ (298 K)	$\Delta G^{\ddagger}$ (298 K)
1	37	23	21	52
2	−12	−27	−29	14
3	47	32	31	72
4	69	55	56	99
5	56	42	40	88
6	−5	−21	−21	30
7	52	39	38	82
8	21	8	8	47

a simple yet representative means of quantifying the abilities of the Pd_n clusters to activate a C-H bond in ethane. The electronic energy of activation ($\Delta E_{elec}^{\ddagger}$) is equivalent to $\Delta U^{\ddagger}$ excluding the zero-point vibrational energy (ZPVE). $\Delta U^{\ddagger}$ is consistently smaller than $\Delta E_{elec}^{\ddagger}$ by ~ 14 kJ/mol mainly because of one less C-H stretching vibrational mode in the TS. $\Delta H^{\ddagger}$ and $\Delta G^{\ddagger}$ at 298 K were calculated using the following equations:

$$\Delta H^{\ddagger} = H(TS) - H\left(Pd_n\right) - H(\text{ethane}) \tag{2}$$

$$\Delta G^{\ddagger} = G(TS) - G\left(Pd_n\right) - G(\text{ethane}) \tag{3}$$

In the above two equations, H(TS) or G(TS) is the lowest possible enthalpy or Gibbs energy of all TS structures for each cluster size n; $H(Pd_n)$ or $G(Pd_n)$ is the lowest possible enthalpy or Gibbs energy of all Pd_n local minimum (LM) structures. Although the internal energy or Helmholtz energy of activation at room temperature is not presented in Fig. 10 or Table 2, they can be easily derived using the following equations:

$$\Delta U^{\ddagger} = \Delta H^{\ddagger} - \Delta(PV)^{\ddagger} = \Delta H^{\ddagger} - RT\Delta n^{\ddagger} = \Delta H^{\ddagger} + RT \tag{4}$$

$$\Delta A^{\ddagger} = \Delta G^{\ddagger} - \Delta(PV)^{\ddagger} = \Delta G^{\ddagger} - RT\Delta n^{\ddagger} = \Delta G^{\ddagger} + RT \tag{5}$$

where $\Delta n^{\ddagger}$ is the change in the number of the moles of gas species ($\Delta n^{\ddagger} = -1$ in a bimolecular reaction) and R is the gas constant. At 298 K, $\Delta U^{\ddagger}$ or $\Delta A^{\ddagger}$ is ~ 2.5 kJ/mol larger than $\Delta H^{\ddagger}$ or $\Delta G^{\ddagger}$, respectively, assuming the ideal behavior of all gas particles.

Pd_4 has the largest 0 K energy of activation (55 kJ/mol) and 298 K enthalpy of activation (57 kJ/mol) among all sizes likely due to its ultrastability. $Pd_{2/6/8}$ have the lowest energy and enthalpy of activation likely due to the large energy decrease when the Pd_n–C_2H_6 reactant complex is formed before overcoming the energy barrier. In particular, sizes 2 and 6 both have negative energy and enthalpy of activation. A negative energy or enthalpy of activation is possible mainly because the energy released in the formation of the Pd_n–C_2H_6 reactant complex

can be greater than the energy barrier this complex overcomes to form the TS structure. Fig. 11 shows that the singlet TS of $Pd_2 + C_2H_6 \rightarrow H{-}Pd_2{-}C_2H_5$ lies 37 kJ/mol below the separate reactants in the singlet state and 12 kJ/mol below the separate reactants in the triplet state. Either way, the energy barrier is negative. The minimum energy path of this reaction starts from the triplet Pd_2 and ethane. In the formation of the Pd_2–C_2H_6 reactant complex, a spin flip can take place (due to the spin–orbit coupling or the spin exchange with nearby species) and all electrons become paired. The singlet Pd_2–C_2H_6 then overcomes a small 4 kJ/mol energy barrier for the hydrogen shift from ethane to Pd_2 and forms the singlet $H{-}Pd_2{-}C_2H_5$.

Negative energy barriers are not a unique phenomenon for $Pd_n + C_2H_6 \rightarrow H{-}Pd_n{-}C_2H_5$. They are also observed in the interaction between ethane and the Pt, Rh, or Ir atomic clusters when the TM_n–C_2H_6 complex (TM = Pt/Rh/Ir) has a lower energy than the TS of the $TM_n + C_2H_6 \rightarrow H - TM_n - C_2H_5$ reaction for selected TM cluster sizes [15, 22, 23].

While Pd_2 has the lowest energy, enthalpy, and Gibbs energy of activation and thus is considered the most active toward ethane, its small atomization energy per atom (29 kJ/mol) and negative second derivative of the atomization energy (− 106 kJ/mol) indicate its very poor thermal stability and a strong tendency to agglomerate or to undergo a disproportionation reaction. Among all studied cluster sizes, Pd_6 and Pd_8 well balance thermodynamic stability and catalytic activity. Their room-temperature Gibbs energies of activation were determined to be 30 and 47 kJ/mol (12*RT* and 19*RT*), respectively, when we considered only the global minima of the Pd cluster and TS for each of these two sizes.

The Gibbs energy of activation may be defined more thoroughly and thereby more accurately via a statistical means assuming the *NPT* condition in which the number of particles (*N*), the pressure (*P*), and temperature (*T*) remain constant. For

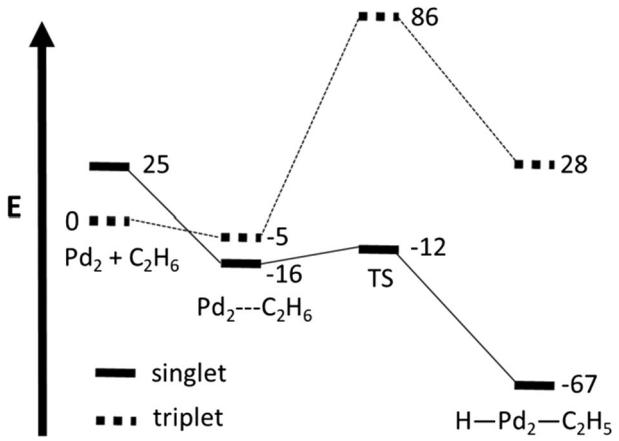

Fig. 11 The CCSD(T) potential energy surface of $Pd_2 + C_2H_6 \rightarrow H{-}Pd_2{-}C_2H_5$ in the singlet (solid line) and triplet states (dotted line). ZPVE is excluded from the potential energy. All numbers are in kJ/mol

example, the Gibbs energy of activation of Pd_n under the isobaric condition may be calculated using the following equation:

$$\Delta G^{\ddagger} = G^{\text{apparent}}(\text{TS}) - G^{\text{apparent}}(Pd_n) - G(\text{ethane}) \quad (6)$$

where G^{apparent} is defined statistically as follows:

$$e^{-\frac{G^{\text{apparent}}}{RT}} = \sum_{i}^{\text{allstructures}} e^{-\frac{G_i}{RT}}$$

Note that $\sum_i^{\text{allstructures}} e^{-\frac{G_i}{RT}}$ provides a reasonable estimate of the thermodynamic contribution of all structures in an ensemble under the constant *PT* condition. Using Eq. 6, $\Delta G^{\ddagger}$ for Pd_{1-8} were determined statistically over the very large number of Pd_n and TS structures studied in this work. The resulting statistical $\Delta G^{\ddagger}$ values are virtually the same as those obtained with Eq. 3 within a negligible discrepancy (0.2 kJ/mol for size 3 and 0.0 kJ/mol for all other sizes). Equations 3 and 5 may differ significantly when there exist multiple Pd_n structures with similar Gibbs energies or when there exist multiple TS structures with similar Gibbs energies. Equation 3 underestimates $\Delta G^{\ddagger}$ in the former case and overestimates $\Delta G^{\ddagger}$ in the latter case.

Two electron-flow mechanisms of $Pd_n + C_2H_6 \rightarrow H{-}Pd_n{-}C_2H_5$

How is the C-H bond in ethane weakened by the Pd clusters? Does the Pd cluster take away C–H bonding electrons or donate electrons to the C–H antibonding orbitals? The calculations of the natural bonding orbital (NBO) charges of the lowest-energy TS structure of the $Pd_n + C_2H_6 \rightarrow H{-}Pd_n{-}C_2H_5$ ($n = 1{-}8$) reaction were carried out at the B3LYP-D3BJ level of theory to reveal the direction of the electron flow between the ethane molecule and the Pd cluster. Table 3 presents the total NBO charge on the Pd cluster in the TS structure. The total charges on the Pd clusters are less than 0.1 in magnitude for all eight sizes. This indicates that the *net* electron flow between the Pd cluster and the ethane molecule is minimal in their interactions.

We further examined the NBO charges on the individual Pd atoms in the Pd_6 and Pd_8 TS structures because they have a large atomization energy per atom (131 and

Table 3 The total charge on Pd_n in the lowest-energy TS structures of the $Pd_n + C_2H_6 \rightarrow H{-}Pd_n{-}C_2H_5$ ($n = 1{-}8$) reaction

n	Charge on Pd_n
1	0.095
2	0.086
3	0.012
4	−0.025
5	0.063
6	0.061
7	0.001
8	−0.010

142 kJ/mol, respectively) and a small enthalpy of activation toward ethane (− 21 and 8 kJ/mol, respectively). The Pd atom partially bonded to the C and H atoms in the TS has a very small NBO charge (− 0.097 and − 0.050 for sizes 6 and 8 respectively). This minimal electron flow in the $Pd_n + C_2H_6 \rightarrow H{-}Pd_n{-}C_2H_5$ reaction contrasts the much larger electron flow between ethane and Ir_8 (a − 0.314 NBO charge on the Ir atom partially bonded to C and H) [15]. For a similar $Rh_8 + C_2H_6$ reaction, the Rh atom partially bonded to C and H also has a large − 0.287 NBO charge [23]. It is clear that the net electron flow is from C_2H_6 to the empty d orbitals of the Ir and Rh clusters but this cannot be the entire story for the Pd clusters. Since the *net* electron flow between Pd_n and C_2H_6 is very small compared to Ir and Rh systems, we conjecture that the Pd clusters weaken the C–H bond of ethane via two mechanisms concurrently. The first involves electron flow from the 4d orbitals of the Pd cluster to the σ* antibonding orbitals in ethane, and the second involves electron flow from the occupied σ bonding orbital of ethane to the empty 4d or 5 s orbitals of the Pd atom(s). The charge transfer between Pd_n and C_2H_6 is small because the Pd_n cluster accepts and donates electrons simultaneously. Despite the minimal net charge transfer between the Pd cluster and ethane, a very important change transpired: some C–H σ bonding electrons become σ* antibonding electrons in ethane and thereby a C–H bond is activated. Fig. 12 provides a rudimentary illustration of these two concurrent electron-flow mechanisms: A Pd_n cluster can donate its 4d electrons to the antibonding orbitals of ethane and meanwhile the same Pd_n cluster can also accept the C–H bonding electrons concurrently. Although the 4d orbitals of the free Pd atom in the ground electronic state are completely occupied, there are partially empty 4d orbitals in a Pd_n cluster that can accommodate electrons from ethane. The NBO charge analysis for other cluster sizes suggests that the same two mechanisms account for the activation of the C–H bond in ethane.

Further NBO charge analysis of the separated ethane and Pd_6 indicates that the shifted H atom, among all atoms, undergoes the most dramatic change in the atomic charge. The NBO charge of H in free ethane is calculated to be 0.22. In the reaction between ethane and Pd_6, the shifted H accepts 0.06 e^- from the Pd cluster and 0.14 e^- from the C_2H_5 group during the formation of the TS structure. This shifted H atom has a very small positive NBO charge (0.02) in the TS structure partly because its Pauling electronegativity is the same as that of Pd (2.2). For Pd_8, the shifted H atom donates 0.01 e^- to the Pd cluster and accepts 0.15 e^- from the C_2H_5 group in the formation of the TS structure. The shifted H atom also has a very small positive NBO charge (0.08) in the TS structure.

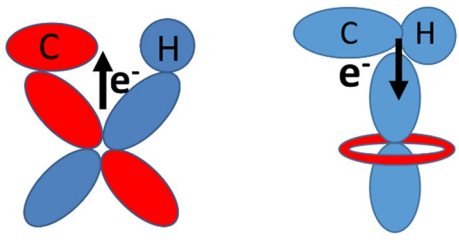

Fig. 12 Two mechanisms account for the Pd_n-activated C–H bond in ethane

Conclusions

We used the CCSD(T)/TZ//B3LYP-D3BJ/DZ dual-level hybrid method to study the various local minima of the Pd atomic clusters (Pd_n) and their abilities to activate a C–H bond in ethane. The global minimum structures of Pd_n ($n = 3 - 8$) are triangular, tetrahedral, triangular bipyramidal, octahedral, pentagonal bipyramidal, and twisted cubic, respectively. The global minima of Pd_n ($n = 1, 3, 7, 8$) are in the singlet electronic state, whereas Pd_n ($n = 2, 4, 5, 6$) are in the triplet electronic state. The shapes of the Pd_n in the lowest-energy TS of $Pd_n + C_2H_6 \rightarrow H{-}Pd_n{-}C_2H_5$ largely resemble the corresponding free Pd_n clusters (with noticeable distortion in the TS structure for sizes 7 and 8). Due to the interaction between ethane and Pd_n that eliminates the (near) degeneracy of molecular orbitals, all lowest-energy TS structures are in the singlet electronic state except for size 7 (which is a triplet). Among the eight cluster sizes studied in this work, size 2 has the lowest energy, enthalpy, and Gibbs energy of activation but it also has poor thermal stability indicated by its small atomization energy and negative second derivative of atomization energy. Size 4 exhibits satisfactory thermal stability, but its ability to activate a C-H bond is significantly poorer than other sizes. Pd_6 and Pd_8 well balance the thermal stability and catalytic ability and thus are likely the ideal sizes for the effective activation of the C–H bonds in ethane. Pd_6 and Pd_8 are considered stable as they both have a large atomization energy per atom: 131 and 142 kJ/mol, respectively. They are considered active toward ethane as their room-temperature Gibbs energies of activation of $Pd_n + C_2H_6 \rightarrow H{-}Pd_n{-}C_2H_5$ are only 30 and 47 kJ/mol ($12RT$ and $19RT$), respectively. In this work, we also quantified the C–H activation abilities of each Pd cluster size in two ways under constant *PT* conditions. One way is to take the difference between the lowest Gibbs energy of the TS structures and the lowest Gibbs energy of the reactants. The other is to take the contribution of all reactant structures and all TS structures into account in a statistical manner under the constant *TP* condition. These two different ways yield virtually the same result because of the lack of (near) degeneracy among the lowest-energy reactants and the lack of (near) degeneracy among the lowest-energy TS structures.

Supplementary Information The online version contains supplementary material available at https://doi.org/10.1007/s11144-023-02475-z.

Acknowledgements Acknowledgment is made to the donors of the American Chemical Society Petroleum Research Fund for partial support of this research. Ge thanks Central Washington University (CWU) for granting his sabbatical leave in Fall 2021. The authors also thank CWU for the access to high-performance computers and particularly Bill Glessner for his technical assistance with high-performance computing.

Funding American Chemical Society Petroleum Research Fund, Grant No. 57389-UR6, Yingbin Ge.

Data availability The authors declare that the data supporting the findings of this study are available within the paper and its Supplementary Information file. Should any raw data files be needed in another format they are available from the corresponding author upon reasonable request.

Declarations

Conflict of interest The authors declare no competing financial or non-financial interest.

References

1. Ethene (Ethylene) http://www.essentialchemicalindustry.org/chemicals/ethene.html
2. Xu Z, Xiao F-S, Purnell SK et al (1994) Size-dependent catalytic activity of supported metal clusters. Nature 372:346–348. https://doi.org/10.1038/372346a0
3. Argo AM, Odzak JF, Lai FS, Gates BC (2002) Observation of ligand effects during alkene hydrogenation catalysed by supported metal clusters. Nature 415:623–626
4. Venegas JM, McDermott WP, Hermans I (2018) Serendipity in catalysis research: boron-based materials for alkane oxidative dehydrogenation. Acc Chem Res 51:2556–2564. https://doi.org/10.1021/acs.accounts.8b00330
5. Shiju NR, Guliants VV (2009) Recent developments in catalysis using nanostructured materials. Appl Catal A Gen 356:1–17. https://doi.org/10.1016/j.apcata.2008.11.034
6. Gaertner CA, van Veen AC, Lercher JA (2013) Oxidative dehydrogenation of ethane: common principles and mechanistic aspects. ChemCatChem 5:3196–3217. https://doi.org/10.1002/cctc.201200966
7. Liu M, Wu J, Hou H (2019) Metal-organic framework (MOF)-based materials as heterogeneous catalysts for C–H bond activation. Chem Eur J 25:2935–2948. https://doi.org/10.1002/chem.201804149
8. Chen KD, Bell AT, Iglesia E (2000) Kinetics and mechanism of oxidative dehydrogenation of propane on vanadium, molybdenum, and tungsten oxides. J Phys Chem B 104:1292–1299
9. Argyle MD, Chen KD, Bell AT, Iglesia E (2002) Effect of catalyst structure on oxidative dehydrogenation of ethane and propane on alumina-supported vanadia. J Catal 208:139–149
10. Heracleous E, Machli M, Lemonidou AA, Vasalos LA (2005) Oxidative dehydrogenation of ethane and propane over vanadia and molybdena supported catalysts. J Mol Catal A Chem 232:29–39
11. Redfern PC, Zapol P, Sternberg M et al (2006) Quantum chemical study of mechanisms for oxidative dehydrogenation of propane on vanadium oxide. J Phys Chem B 110:8363–8371. https://doi.org/10.1021/jp056228w
12. Russell J, Zapol P, Král P, Curtiss LA (2012) Methane bond activation by Pt and Pd subnanometer clusters supported on graphene and carbon nanotubes. Chem Phys Lett 536:9–13. https://doi.org/10.1016/j.cplett.2012.03.080
13. Kulkarni A, Lobo-Lapidus RJ, Gates BC (2010) Metal clusters on supports: synthesis, structure, reactivity, and catalytic properties. Chem Commun 46:5997–6015. https://doi.org/10.1039/c002707n
14. Uzun A, Dixon DA, Gates BC (2011) Prototype supported metal cluster catalysts: Ir_4 and Ir_6. ChemCatChem 3:95–107. https://doi.org/10.1002/cctc.201000271
15. Ge Y, Jiang H, Kato R, Gummagatta P (2016) Size and site dependence of the catalytic activity of iridium clusters toward ethane dehydrogenation. J Phys Chem A 120:9500–9508. https://doi.org/10.1021/acs.jpca.6b09882
16. Cui Q, Musaev DG, Morokuma K (1998) Molecular orbital study of H_2 and CH_4 activation on small metal clusters. 2. Pd_3 and Pt_3. J Phys Chem A 102:6373–6384. https://doi.org/10.1021/jp982273a
17. Ciebien JF, Cohen RE, Duran A (1998) Catalytic properties of palladium nanoclusters synthesized within diblock copolymer films: hydrogenation of ethylene and propylene. Supramol Sci 5:31–39
18. Bell AT (2003) The impact of nanoscience on heterogeneous catalysis. Science 299:1688–1691
19. Keränen J, Auroux A, Ek S, Niinistö L (2002) Preparation, characterization and activity testing of vanadia catalysts deposited onto silica and alumina supports by atomic layer deposition. Appl Catal A Gen 228:213–225. https://doi.org/10.1016/S0926-860X(01)00975-9
20. Adlhart C, Uggerud E (2005) C–H activation of alkanes on Rh_n^+ ($n = 1 - 30$) clusters: size effects on dehydrogenation. J Chem Phys 123:214709

21. Adlhart C, Uggerud E (2007) Mechanisms for the dehydrogenation of alkanes on platinum: Insights gained from the reactivity of gaseous cluster cations, Pt_n^+, $n = 1 - 21$. Chem Eur J 13:6883–6890. https://doi.org/10.1002/chem.200700501
22. Shore TC, Mith D, DePrekel D et al (2013) A B3LYP study on the C–H activation in propane by neutral and +1 charged low-energy platinum clusters with 2–6 atoms. React Kinet Mech Catal 109:315–333. https://doi.org/10.1007/s11144-013-0572-3
23. Ge Y, Le A, Marquino GJ et al (2019) Tools for prescreening the most active sites on Ir and Rh clusters toward C–H bond cleavage of ethane: NBO charges and wiberg bond indexes. ACS Omega 4:18809–18819. https://doi.org/10.1021/acsomega.9b02813
24. Tan C, Liu H, Qin Y et al (2023) Correlation between the properties of surface lattice oxygen on NiO and its reactivity and selectivity towards the oxidative dehydrogenation of propane. ChemPhysChem 24:e202200539. https://doi.org/10.1002/cphc.202200539
25. Argo AM, Odzak JF, Gates BC (2003) Role of cluster size in catalysis: Spectroscopic investigation of γ-Al_2O_3-supported Ir_4 and Ir_6 during ethene hydrogenation. J Am Chem Soc 125:7107–7115. https://doi.org/10.1021/ja027741f
26. Nasr Azadani F, Fatemi S, Salehi Ardali N (2022) Kinetic modeling and optimization of the operating conditions of benzene alkylation with ethane on PtH-ZSM-5 catalyst. React Kinet Mech Catal 135:669–685. https://doi.org/10.1007/s11144-022-02188-9
27. Xie Q, Miao C, Lei T et al (2021) Dehydrogenation of ethane assisted by CO_2 over Y-doped ceria supported Au catalysts. React Kinet Mech Catal 132:417–429. https://doi.org/10.1007/s11144-020-01910-9
28. Eslek Koyuncu DD (2021) Investigation of the effect of microwave heated reactor on ethane dehydrogenation over KIT-6 supported catalysts. React Kinet Mech Catal 132:379–399. https://doi.org/10.1007/s11144-021-01928-7
29. Botková Š, Čapek L, Setnička M et al (2016) VO_x species supported on Al_2O_3–SBA-15 prepared by the grafting of alumina onto SBA-15: structure and activity in the oxidative dehydrogenation of ethane. React Kinet Mech Catal 119:319–333. https://doi.org/10.1007/s11144-016-1036-3
30. Barthos R, Novodárszki G, Valyon J (2017) Heterogeneous catalytic Wacker oxidation of ethylene over oxide-supported Pd/VO_x catalysts: the support effect. React Kinet Mech Catal 121:17–29. https://doi.org/10.1007/s11144-016-1123-5
31. Ferguson GA, Mehmood F, Rankin RB et al (2012) Exploring computational design of size-specific subnanometer clusters catalysts. Top Catal 55:353–365. https://doi.org/10.1007/s11244-012-9804-4
32. Vajda S, Pellin MJ, Greeley JP et al (2009) Subnanometre platinum clusters as highly active and selective catalysts for the oxidative dehydrogenation of propane. Nat Mater 8:213–216. https://doi.org/10.1038/nmat2384
33. Gaffney AM, Mason OM (2017) Ethylene production via oxidative dehydrogenation of ethane using M1 catalyst. Catal Today 285:159–165. https://doi.org/10.1016/j.cattod.2017.01.020
34. Sattler JJHB, Ruiz-Martinez J, Santillan-Jimenez E, Weckhuysen BM (2014) Catalytic dehydrogenation of light alkanes on metals and metal oxides. Chem Rev 114:10613–10653. https://doi.org/10.1021/cr5002436
35. Zhang W, Wang L (2011) The effect of cluster thickness on the adsorption of CH_4 on Pd_n. Comput Theor Chem 963:236–244. https://doi.org/10.1016/j.comptc.2010.10.027
36. Xiao L, Wang L (2007) Methane activation on Pt and Pt_4: a density functional theory study. J Phys Chem B 111:1657–1663. https://doi.org/10.1021/jp065288e
37. Foster JP, Weinhold F (1980) Natural hybrid orbitals. J Am Chem Soc 102:7211–7218. https://doi.org/10.1021/ja00544a007
38. Reed AE, Weinhold F (1983) Natural bond orbital analysis of near-Hartree–Fock water dimer. J Chem Phys 78:4066–4073. https://doi.org/10.1063/1.445134
39. Wiberg KB (1968) Application of the pople-santry-segal CNDO method to the cyclopropylcarbinyl and cyclobutyl cation and to bicyclobutane. Tetrahedron 24:1083–1096. https://doi.org/10.1016/0040-4020(68)88057-3
40. Harper LK, Shoaf AL, Bayse CA (2015) Predicting trigger bonds in explosive materials through wiberg bond index analysis. ChemPhysChem 16:3886–3892. https://doi.org/10.1002/cphc.201500773
41. Mayer I (2007) Bond order and valence indices: a personal account. J Comput Chem 28:204–221. https://doi.org/10.1002/jcc.20494

42. Davis JBA, Shayeghi A, Horswell SL, Johnston RL (2015) The Birmingham parallel genetic algorithm and its application to the direct DFT global optimisation of Ir_N (N = 10–20) clusters. Nanoscale 7:14032–14038. https://doi.org/10.1039/C5NR03774C
43. Davis JBA, Horswell SL, Johnston RL (2014) Global optimization of 8–10 atom Palladium-Iridium nanoalloys at the DFT Level. J Phys Chem A 118:208–214. https://doi.org/10.1021/jp408519z
44. Shayeghi A, Götz DA, Davis JBA et al (2015) Pool-BCGA: a parallelised generation-free genetic algorithm for the ab initio global optimisation of nanoalloy clusters. Phys Chem Chem Phys 17:2104–2112. https://doi.org/10.1039/c4cp04323e
45. Jäger M, Schäfer R, Johnston RL (2018) First principles global optimization of metal clusters and nanoalloys. Adv Phys X 3:1516514. https://doi.org/10.1080/23746149.2018.1516514
46. Nava P, Sierka M, Ahlrichs R (2003) Density functional study of palladium clusters. Phys Chem Chem Phys 5:3372–3381. https://doi.org/10.1039/B303347C
47. Khatun M, Majumdar RS, Anoop A (2019) A global optimizer for nanoclusters. Front Chem. https://doi.org/10.3389/fchem.2019.00644
48. Kalita B, Deka RC (2007) Stability of small Pd_n (n = 1–7) clusters on the basis of structural and electronic properties: a density functional approach. J Chem Phys 127:244306. https://doi.org/10.1063/1.2806993
49. Rogan J, Garcia G, Valdivia JA et al (2005) Small Pd clusters: a comparison of phenomenological and ab initio approaches. Phys Rev B 72:115421. https://doi.org/10.1103/PhysRevB.72.115421
50. Luo C, Zhou C, Wu J et al (2007) First principles study of small palladium cluster growth and isomerization. Int J Quantum Chem 107:1632–1641. https://doi.org/10.1002/qua.21315
51. Becke AD (1993) Density-functional thermochemistry. III. The role of exact exchange. J Chem Phys 98:5648–5652
52. Lee C, Yang W, Parr R (1988) Development of the Colle-Salvetti correlation-energy formula into a functional of the electron density. Phys Rev B 37:785–789
53. Stephens PJ, Devlin FJ, Chabalowski CF, Frisch MJ (1994) Ab initio calculation of vibrational absorption and circular dichroism spectra using density functional force fields. J Phys Chem 98:11623–11627
54. Grimme S, Ehrlich S, Goerigk L (2011) Effect of the damping function in dispersion corrected density functional theory. J Comput Chem 32:1456–1465. https://doi.org/10.1002/jcc.21759
55. Hay PJ, Wadt WR (1985) Ab initio effective core potentials for molecular calculations. Potentials for K to Au including the outermost core orbitals. J Chem Phys 82:299–310
56. Ehlers AW, Bohme M, Dapprich S et al (1993) A set of f-polarization functions for pseudo-potential basis sets of the transition metals Sc–Cu, Y–Ag and La–Au. Chem Phys Lett 208:111–114
57. Hehre WJ, Ditchfield R, Pople JA (1972) Self-consistent molecular-orbital methods.12. Further extensions of Gaussian-type basis sets for use in molecular-orbital studies of organic-molecules. J Chem Phys 56:2257–2261
58. Hariharan PC, Pople JA (1973) The influence of polarization functions on molecular orbital hydrogenation energies. Theo Chim Acta 28:213–222
59. Liu W, Ren Z, Bosse AT et al (2018) Catalyst-controlled selective functionalization of unactivated C–H bonds in the presence of electronically activated C–H bonds. J Am Chem Soc 140:12247–12255. https://doi.org/10.1021/jacs.8b07534
60. Glendening ED, Reed AE, Carpenter JE, Weinhold. F NBO Version 3.1
61. Frisch MJ, Trucks GW, Schlegel HB, et al (2009) Gaussian 09, Revision D.1
62. Frisch MJ, Trucks GW, Schlegel HB, et al (2016) Gaussian 16, Revision A.3
63. Moore CE (1952) Atomic Energy Levels. Washington D.C.
64. Zhang W, Ge Q, Wang L (2003) Structure effects on the energetic, electronic, and magnetic properties of palladium nanoparticles. J Chem Phys 118:5793–5801. https://doi.org/10.1063/1.1557179
65. Lee S, Bylander DM, Kleinman L (1989) Pd_2: a dimer with two Kohn-Sham triplet ground states. Phys Rev B Condens Matter 39:4916–4920. https://doi.org/10.1103/physrevb.39.4916
66. Ganteför G, Gausa M, Meiwes-Broer K-H, Lutz HO (1990) Photoelectron spectroscopy of silver and palladium cluster anions. Electron delocalization versus localization. J Chem Soc, Faraday Trans 86:2483–2488. https://doi.org/10.1039/FT9908602483
67. Ho J, Ervin KM, Polak ML et al (1991) A study of the electronic structures of Pd_2^- and Pd2 by photoelectron spectroscopy. J Chem Phys 95:4845–4853. https://doi.org/10.1063/1.461702
68. Franck EU (1989) J. D. Cox, D. D. Wagman, V. A. Medvedev: CODATA—key values for thermodynamics, aus der Reihe: CODATA, series on thermodynamic properties. Hemisphere Publishing Corporation, New York, Washington, Philadelphia, London, Wiley

69. Huber KP, Herzberg G (1979) Constants of diatomic molecules. Molecular spectra and molecular structure: IV. Constants of diatomic molecules. Springer, Boston, pp 8–689
70. Valerio G, Toulhoat H (1996) Local, gradient-corrected, and hybrid density functional calculations on Pd_n clusters for n = 1–6. J Phys Chem 100:10827–10830. https://doi.org/10.1021/jp960356q
71. Seminario JM, Zacarías AG, Castro M (1997) Systematic study of the lowest energy states of Pd, Pd_2, and Pd3. Int J Quantum Chem 61:515–523
72. Balasubramanian K (1989) Ten low-lying electronic states of Pd_3. J Chem Phys 91:307–313. https://doi.org/10.1063/1.457518